https://doi.org/10.5194/egusphere-2023-234
Preprint. Discussion started: 15 February 2023

Simulated Long-term Evolution of the Thermosphere during the Holocene: 2. Circulation and Solar Tides

Xu Zhou[1,3], Xinan Yue[1,2,3], Yihui Cai[1,2,3], Zhipeng Ren[1,2,3], Yong Wei[1,2,3], Yongxin Pan[1,2,3]

[1]Key Laboratory of Earth and Planetary Physics, Institute of Geology and Geophysics, Chinese Academy of Sciences, Beijing, 100029, China

[2]College of Earth and Planetary Sciences, University of Chinese Academy of Sciences, Beijing, 100029, China

[3]Beijing National Observatory of Space Environment, Institute of Geology and Geophysics, Chinese Academy of Sciences, Beijing, 100029, China

Correspondence to: Xinan Yue (yuexinan@mail.iggcas.ac.cn)

Abstract. On timescales longer than the solar cycle, long-term changes in CO2 concentration and geomagnetic field have the potential to affect thermospheric dynamics. In this paper, we investigate the thermospheric dynamical response to these two factors during the Holocene, using two sets of ~12,000-yr control runs by the coupled thermosphere-ionosphere model, GCITEM-IGGCAS. The main results indicate that increased/decreased CO2 will enhance/weaken the thermospheric circulation throughout the Holocene, but this effect is nonlinear. The cooling effect of CO2 in the thermosphere further provides plausible conditions for atmospheric tidal propagation and increases the thermospheric tidal amplitude. Geomagnetic variations induce hemispheric asymmetrical responses in the thermospheric circulation. Large changes in the circulation occur at high latitudes in the hemisphere with distant magnetic poles drift, inferring a crucial role of geomagnetic non-dipole variations in circulation changes. A positive correlation between the diurnal migrating tide (DW1) and geomagnetic dipole moment is revealed for the first time. The amplitude of DW1 in temperature will increase by ~1–3 K for each 1×10^{22} Am^2 increase in dipole moment.

1 Introduction

The main external energy input to the terrestrial thermosphere is solar radiation, particularly in the extreme ultraviolet (EUV) band. The solar-driven circulation manifests as the flow across the isobars, in contrast to the geostrophic flow that dominates in the middle and lower atmosphere (Forbes, 2007). This is because the Coriolis force is much smaller than the pressure gradient term for the typical terrestrial thermosphere. Under absorption of solar daily-cyclic forcing, the atmosphere also induces the solar tides, which refers to global-scale perturbations in atmospheric parameters with periods and zonal wave numbers that are harmonics of a day and a zonal cycle. In addition to the local absorption of EUV radiation as the major source, the solar tides in the thermosphere also come from upward propagating waves excited in the middle and lower atmosphere, including the infrared absorption by tropospheric H2O and ultraviolet absorption by stratospheric O3 (Forbes and Zhang, 2022). Thus, the level of solar activity is expected to have a key impact on the dynamical variability in the thermosphere

https://doi.org/10.5194/egusphere-2023-234
Preprint. Discussion started: 15 February 2023

(Oberheide et al., 2009; Sun et al., 2022). However, when inspecting on time scales longer than the solar cycle, the influence from other secular variables, such as long-term changes in CO2 concentration and main geomagnetic fields, should not be ignored. It is then natural to ask how and to what extent these factors act on the thermospheric dynamics on long-term time scales, e.g., since the Holocene.

CO2 plays a significant role in cooling the thermosphere, in contrast to the warming effect in the troposphere (Laštovička et al., 2006; Solomon et al., 2018). Since the first prediction by Roble & Dickinson (1989), many observational evidences and simulation experiments have been subsequently proposed to support the CO2 cooling effect using modern techniques and advanced models (Akmaev & Fomichev, 2000; Akmaev et al., 2006; Marsh et al., 2013; Ogawa et al., 2014; Qian et al., 2011; 2006; Solomon et al., 2015; Zhang et al. 2016). A well-established consensus is that every 10 ppm increase in CO2 concentration will result in a ~1–3K decrease in global-mean temperature in the thermosphere (e.g. Solomon et al., 2018). As the issue of increasing CO2 becomes urgent (IPCC, 2014), have also worked to elucidate the concomitant effects on the upper atmosphere (Zhou et al., 2022), and one of which is the thermospheric dynamics. Using the GAIA (Ground-to-topside Atmosphere Ionosphere model for Aeronomy) simulation, Liu et al. (2020) suggested that the doubling of CO2 concentration should strengthen thermospheric meridional circulation, enhance diurnal migrating tide, and weaken semidiurnal migrating tide. Kogure et al. (2022) further analyzed the underlying mechanism of the thermospheric zonal mean wind response, suggesting that the ion drag, molecular viscosity, and meridional pressure gradient forces as the three main factors are in the combined modulation. However, the impact of CO2 on the long-term evolution of the thermospheric dynamics during the Holocene is still poorly inderstood.

The secular variation of the geomagnetic field would produce considerable changes in the thermosphere temperature other than the CO2 effect. Although the geomagnetic variation does not act directly on the neutral atmosphere, it affects ion motion and thus ionospheric behavior (Cai et al., 2019; Elias et al., 2022; Yue et al., 2018; Zossi et al., 2018), which are coupled to the neutral atmosphere via ion-neutral collisions. The strength of the geomagnetic field determines the gyrofrequency and the ionospheric conductivity, thus influencing the Joule heating power and $\mathbf{E}\times\mathbf{B}$ drift velocities (Cnossen et al., 2012; Zhou et al., 2021). The geomagnetic tiled angle controlling the geographic distribution of the Joule heating should produce further changes in temperature and neutral winds (Cnossen & Richmond, 2012). Cnossen (2014) reported that the geomagnetic variation over the last century could cause a ~±10K change in the thermosphere temperature regionally, comparable to the –8K decrease in global temperature due to increased CO2 over the same period. Analyses of recent decades (Cnossen et al., 2020) and projections in the coming decades (Cnossen et al., 2022) about the thermospheric climate change confirm the importance of the geomagnetic variation, although accelerating CO2 growth still plays a dominant role. Since the geomagnetic field has

https://doi.org/10.5194/egusphere-2023-234
Preprint. Discussion started: 15 February 2023

undergone a more complex evolution during the Holocene than in the present century (Korte et al., 2011), the impact on the evolution of thermospheric dynamics is expected to be more dramatic and therefore worth investigating.

The aim of the present study is to discuss the scenario of thermospheric dynamic changes due to the long-term changes in CO2 concentration and geomagnetic field during the Holocene. This paper is organized as follows: Section 2 will briefly introduce the numerical simulation settings. Section 3 will show the main results of the simulations, then Section 4 discuss the scientific key points. In the end, a short summary is given in Section 5.

2 Model Description and Settings

Attempting to understand the long-term evolution of thermospheric dynamics affected by these two factors in the Holocene, we designed long-term time-slice simulations based on the Global Coupled Ionosphere-Thermosphere-Electrodynamics Model developed at the Institute of Geology and Geophysics, Chinese Academy of Sciences (GCITEM-IGGCAS, Ren et al., 2009, 2010, 2011, 2020). Detailed model description and settings are referred to Yue et al. (2022) and Cai et al. (2023), which have carefully investigated the global thermal structure and density profile of the thermosphere and ionosphere, respectively. Here, we give a briefly introduction to restate and to add key information. This 3-dimensional coupled thermosphere-ionosphere model self-consistently solves the global thermospheric and ionospheric behavior in the altitudinal coordinate, covering altitudes from 90 km to 600 km. The ionospheric electro-dynamics is solved on the provided geomagnetic field configuration using magnetic apex coordinates (Richmond, 1995) based on a set of spherical harmonic coefficients. The calculation scheme requires the geomagnetic field to be dipole-dominated, so the situation of geomagnetic reversal is difficult to portray. The high-latitude electric potential and electric fields are specified by the empirical model of Weimer-96 (Weimer, 1996), which is driven by the hemispheric power (HP), solar wind speed (SWS), interplanetary magnetic field (IMF), and cross-polar cap potential (CPCP). At the lower boundary at 90 km, migrating tide in neutral temperature and density are given by the Global Scale Wave Model (GSWM), while neutral winds are self-consistently calculated. Non-migrating tides are not included in this study. The solar EUV radiation is described by the empirical model EUVAC (Richards et al., 1994), which is driven by the proxy of solar flux at 10.7 cm (F10.7). The CO2 cooling is calculated under the assumption of the nonlocal thermodynamic equilibrium (NLTE) with a cooling-to-space approximation assumed. In this model, the CO2 level is specified by a given value for a fixed time under the assumption of diffusive equilibrium. This calculation formula follows Roble et al. (1988), and is also adopted by other thermosphere-ionosphere coupled models, such as NCAR-TIEGCM (Qian et al., 2017).

To diagnose the long-term effects of CO2 and geomagnetic field variations on the thermospheric dynamics, two control runs (CR1 and CR2) were performed under perpetual solar minimum and geomagnetic quiet condition, which correspond to the

https://doi.org/10.5194/egusphere-2023-234
Preprint. Discussion started: 15 February 2023

CR2 and CR1 in the Yue et al. (2022) and Cai et al. (2023). The driving parameters in Weimer-96 model are set as HP = 10GW, SWS = 300 m/s, IMF By = 0 nT, IMF Bz = –0.5 nT, and CPCP = 20 kV for both cases, representing the extreme geomagnetically quiet condition of Kp = ~0.3. To eliminate the impact of solar variation, each case was performed under solar minimum, correspondingly the F10.7 setting to be constant of 87sfu (solar flux unit, 1 sfu = 10^{-22} W m^{-2} Hz^{-1}). In CR1, realistic CO2 from a combined dataset drives the GCITEM-IGGCAS model with a fixed configuration of geomagnetic fields. Hence, the simulated variability of the thermosphere is derived exclusively from the CO2 changes. The CO2 dataset consists of three components: (1) Estimation from the ice cores recorded air composition in the interval of ~80,000 yrs before ~1650 with a rough resolution of ~100 yrs during the Holocene (Lüthi et al., 2008). (2) Measurement in ice with high precision back to 2000 yrs before the present (MacFarling Meure et al., 2006). (3) Modern atmospheric measurement at Mauna Loa Observatory, Hawaii, since 1958 (Keeling et al., 1995). In CR2, the CO2 level is fixed to be 270 ppm, corresponding to the averaged value during the Holocene, while the geomagnetic fields are set to be varied with time. The specified geomagnetic field before 1900 is provided by the CALS10k.2 model developed by Constable et al. (2016), which is based on the archeo-magnetic and lake sediment data. Generally, this model roughly has spherical harmonics to degree and order of 10, and cubic B-splines parameterization is implemented with knots positioned every 40 yrs. After 1900, the geomagnetic fields are described by the International Geomagnetic Reference Field (IGRF) model (Alken et al., 2021). This model is based on the modern magnetic observations to describe the spatial distribution of geomagnetic fields by the spherical harmonic degree and order of 13 with the time resolution of 5 yrs. Both cases were run every 100 yrs in the period of 9455 BC to 1945 AD, and an additional run of 2015 AD was for the contemporary condition. Particularly, pre-runs of 15 days were performed as spin-up preparation to eliminate the influence from the initial conditions, and the outputs in the last day were used for analysis. Each case was running in two seasons, March and June, with the aim of discussing the seasonal dependence of the thermospheric dynamical response..

3 Results

3.1 CO2 effect

According to the CR1 results, Figure 1 illustrates the changes in zonal-mean winds due to increased CO2 from 1945 to 2015 (310 to 400 ppm), exemplifying how the changes in CO2 act on the thermospheric circulation. Figures 1b–1d show the strengthening of the thermospheric circulation in March, mainly including enhanced equatorward flow from the north and south poles, accelerated eastward flow at mid- and low-latitudes latitudes, and increased downward/upward movement in the upper/lower thermosphere. The acceleration of the eastward zonal and equatorial meridional winds winds is about ~1–2 m/s when CO2 is increased by ~90 ppm. The CO2 acceleration effect of the thermosphreic circulation is also evident in June. Figures 1f–1h show the enhanced summer-to-winter prevailing wind and corresponding increased westward/eastward zonal wind in the summer/winter hemisphere due to the Coriolis force. The vertical winds also show a downward increase in the

https://doi.org/10.5194/egusphere-2023-234
Preprint. Discussion started: 15 February 2023

upper thermosphere, while the slight increase in the lower thermosphere disappears around the winter pole. Compared to the wind change in March, the accelerated thermospheric winds in June achieve ~2–3 m/s in zonal and meridional, and a few cm/s in vertical. Our simulation gives a reasonable and convincing result compared to the GAIA simulation of Liu et al. (2020), which shows an increase in the meridional winds of 5–15 m/s when CO2 increases by 345 ppm.

Examining the CO2 effect on the thermospheric circulation throughout the Holocene, Figure 2 illustrates the time evolution of changes in meridional wind versus latitudes in the CR2 simulation. The chosen height of ~197 km is where the changes in the meridional wind are significant as shown in Figure 1. The result for the beginning year (–9455) have been subtracted in order to show the CO2 effect more intuitively. The corresponding CO2 variation is plotted in red-solid line, which is also subtracted the CO2 level in the beginning year (264 ppm). Changes in the meridional circulation are obviously highly correlated with CO2 variation, and become much more significant since ~1800 when the increase in CO2 was much larger due to the industrial revolution. The correlation coefficient is generally over ±0.99 at most latitudes. During the equinox season, the meridional circulation varied to be much equatorward/poleward due to the increase/decrease of CO2. As for the solstice season, the CO2 effect manifests to be acceleration/deceleration of the summer-to-pole circulation. For the past over 10,000 years before ~1800, the change in meridional circulation velocity in March and June only fluctuated by ∓0.4–±0.1 m/s and –0.6–0.2 m/s, respectively. However, in the last 200 years, the CO2-induced changes in meridional wind could reach more than 1 m/s. Figure 3 further analyses the CO2 effect on the thermospheric dynamics, choosing the averaged zonal circulation as a proxy. The results show that CO2 enhances the eastward flow at the equator during March, rather than being strictly linear. The growth of the accelerated eastward flow becomes small as CO2 increases. Linear regressions show a change of 0.012 m/s in the thermospheric equatorial zonal flow per ppm CO2 increase, and the parabolic fit should be in good agreement with the simulated data. The parabolic fitting obviously indicates that the rate of change of the thermospheric circulation slows down at the present CO2 level. A similar nonlinear effect is also manifested in the June zonal circulation (Figure 3c).

As for the solar tidal response to the CO2 variation during the Holocene, Figure 4 illustrates the time evolution of diurnal migrating tide in temperature (DW1-T) at ~240 km, which is the major tidal component in the thermosphere. The DW1-T tidal amplitude is positively correlated with CO2 changes, manifesting as increasing by ~10 K compared with the beginning year (-9455) during March when the CO2 level achieve 400 ppm in the modern era, particularly maximizing at the equatorial and low-latitude region. From 8000 BC to 4000 BC, when the CO2 level was low throughout the Holocene, the DW1-T amplitude also decreased slightly. The specified DW1-T amplitude at the lower boundary in March is a maximum of ~16 K at the equator and two secondary peaks of ~7 K at ±35°. As for the DW1-T at the lower boundary in June, the strength is about ~1/2 of that during March. Correspondingly, the changes in the thermospheric DW1-T amplitude in the modern era are slightly over 2 K,

https://doi.org/10.5194/egusphere-2023-234
Preprint. Discussion started: 15 February 2023

only ~1/4 than that in March. The maximum change is found at mid-latitudes in the winter hemisphere, rather than the equator. The latitudinal difference in the DW1-T changes is contrary with the DW1-T time tendency, which generally maximizes in the summer hemisphere (Gu & Du, 2018).

3.2 Geomagnetic field effect

The geomagnetic field effect on the thermospheric circulation is regional and complicated, unlike the global effect of CO2. Figure 5 exemplified the thermospheric circulation in the present era in the CR2 simulation, and manifested how the circulation changed over the past 70 years due to the geomagnetic variation. The thermospheric winds generally flow across the isotherm due to the pressure gradient force and can maximize over 100 m/s around the terminator. The auroral heating modulates the solar-driven winds and decreases the poleward flow at high- and mid-latitudes. Figure 5b shows that the geomagnetic variation from 1945 to 2015 alters the geographic distribution of temperature in March, notably at high latitudes (~±15 K) and not negligibly at mid- and low-latitudes (±5 K). Correspondingly, the change in horizontal neutral winds could exceed 30 m/s at high latitudes and around the dusk sector. The changes in temperature and wind induced by the geomagnetic field are smaller in June than that in March, which is about ±10 K/±3 K at high/mid-low latitudes for temperature and maximizes ~20 m/s for horizontal winds. The circulation change in the northern hemisphere is much larger in the southern hemisphere, regardless during March or June. The horizontal wind changes in the southern hemisphere are generally smaller by 10–20 m/s than that in the northern hemisphere, and the temperature change is smaller by 5–10 K. The hemisphere difference is coincident with the asymmetrical change in the geomagnetic poles. The northern magnetic pole shifted 12° and 76° in latitude and longitude, respectively. However, the southern magnetic pole drifted by merely 4° and 7° in latitude and longitude, respectively.

In addition, Figures 5b and 5d show that the geomagnetic variation during the period 1945–2015 induced different temperature responses during the daytime/nighttime at mid- and low-latitudes. This local-time-dependent effect is further examined in Figure 6 and Figure 7 for the month of March and June, respectively. Figure 6a illustrates the local-time dependence of temperature changes due to the geomagnetic variation with respect to the beginning year of 9455 BC, when the dipole moment of the geomagnetic field underwent a minimum period. During the daytime, the average temperature at low-latitude was generally higher than in 9455 BC for most of the time, except for 4900 BC and 4700 BC. The changed magnitude varied from –2 K to 9 K. In contrast, the nighttime temperature change is negative compared to 9455 BC since 3100 BC, and ranges from –7 K to +6K before 3100 BC. We then deduced the day-night differences in the temperature response at mid- and low-latitudes and illustrated them in comparison with the strength of the geomagnetic dipole moment in Figure 6b. The results show an obviously positive correlation between the day-night differences and the geomagnetic dipole moment, indicating that a stronger geomagnetic dipole moment would induce larger day-night temperature differences in the thermosphere at mid-to-low latitudes

https://doi.org/10.5194/egusphere-2023-234
Preprint. Discussion started: 15 February 2023

in March, thereby exacerbating the prevailing day-to-night flow. During the whole simulation period in the Holocene, the day-night difference in temperature caused by the geomagnetic variation can vary up to ~15–20K. The fluctuation magnitude is about 5% concerning the day-night temperature difference in the thermosphere is generally 300–400K. Meanwhile, the geomagnetic dipole moment varies more than 40%. As for the case of June, the positive correlation is not valid for all latitudes and becomes more complicated. As the dipole moment increases, the average temperature at low-latitudes decreases for both daytime and nighttime. The change in the day-night temperature difference is weaker than that in March. Around the equator and in the southern mid-latitudes, the day-night difference in temperature decreases while the geomagnetic dipole moment increases, such as during 8000–6600 BC and 2600 BC–1600 AD.

As mentioned above, the daytime temperature responses in the thermosphere differed from that of the nighttime due to the geomagnetic variation, suggesting that the tidal response should also be affected, especially during March. Figure 8 then examines the thermospheric tidal response to the geomagnetic variation during the Holocene in the CR2 simulation, including the diurnal and semidiurnal migrating tides in temperature (DW1-T and SW2-T). These two major tidal components respond differently to the geomagnetic variation. The strength of DW1-T is positively correlated with the geomagnetic dipole moment. When the dipole moment intensity becomes ~40% larger than at the beginning of the simulation, the amplitude of DW1-T increases correspondingly by ~10 K. However, the SW2-T around the equator is negatively correlated to the geomagnetic dipole moment, while at mid-latitudes it is positively correlated. The strength of SW2-T response to the geomagnetic variation is much smaller than that of DW1-T, and ranges within ~±2K throughout the simulation period in the Holocene. Figure 9 further diagnoses the relationship between the thermospheric migrating tides and the geomagnetic dipole moment for different thermospheric altitudes versus latitudes. A linear regression between the tidal amplitude and geomagnetic dipole moment is calculated. Figures 9a and 9b illustrate the estimated coefficient for the linear regression in the altitude-latitude plane, with regions where the absolute value of the correlation coefficient is less than 0.6 being masked. The results show that as the geomagnetic dipole moment increases per $10^{22}AM^2$ the thermospheric DW1-T in March would enhance by 1–3 K, with two maximums around ±30°–40°. The response of SW2-T is much smaller and insignificant. At the equator, the increase in geomagnetic dipole moment by $10^{22}AM^2$ would lessen the SW2-T amplitude merely ~0.3 K. A slight enhancement of SW2-T due to the increase in geomagnetic dipole moment could be found in the upper thermosphere at mid-latitudes, while the growth rate is only ~0.4 $K/10^{22}AM^2$.

4 Discussion

In this paper, two control runs, CR1 and CR2, were conducted to examine the response of thermospheric dynamics to long-term changes in CO2 and geomagnetic field during the last 12,000 years of the Holocene. The CO2 effect was revealed as an enhancement of the general circulation with increasing CO2 levels (Figure 1–2), which agreed with the result of Liu et al. (2020). Rind et al. (1990) also found that an increase in CO2 similarly enhanced the mesospheric circulation. Both of them suggested that the increased eddy forcing and gravity waves (GWs) should play an important role. However, the GCITEM-IGGCAS model does not involve a parameterization scheme for GWs because the GWs mainly affect the mean flow in the mesosphere rather than in the thermosphere. Therefore, the changes in the circulation caused by CO2 variations in our results cannot be attributed to GWs. The interpretation by Kogure et al. (2022) should be responsible for the fact that the changes in ion drag, molecular viscosity, and meridional pressure gradient forces are in the combined modulation. An interesting founding is that the CO2 increase does not linearly accelerate the circulation and tends to be "saturated" as shown in Figure 3. The plausible explanation is the molecular viscosity is non-linearly related to the temperature. As for the tidal response to the CO2 effect, the DW1 amplitude is positively correlated with CO2 variation (Figure 4). A reasonable deduction is that the decreased viscosity due to the enhanced CO2 cooling should be less likely to dissipate tidal propagation from below. The latitudinal structure of the DW1 response to CO2 differs from that of Liu et al. (2020), partly because their results mixed the influences of changes in tidal sources from below, whereas our results reflected the internal thermospheric responses.

Figure 5 illustrated an asymmetric response in circulation to the geomagnetic variation. The change in neutral winds was larger in the hemisphere with a more distant geomagnetic pole shift. Given the variation in the dipole component of the geomagnetic field is hemispherical symmetric, it could logically infer that the hemisphere difference in circulation is contributed by the variation of the non-dipole component. The neutral temperature change due to geomagnetic variation has a similar pattern to the ion temperature in Cnossen et al. (2014), which is also manifested to decrease around the daytime equatorial ionization anomaly (EIA) peaks. A possible causal linkage could be proposed that the geomagnetic variation affected the equatorial plasma drift velocity, and then redistributed the electron density around the EIA region. As the electron density becomes large/small the electron temperature changed conversely. The ion temperature change then should be more or less related to the electron temperature change. Generally, the smaller strength of the geomagnetic fields would induce stronger equatorial **E**×**B** drift and thus increase the electron density at the EIA peaks, and Yue et al. (2022) confirmed such a relationship. During the nighttime, the equatorial drift tended to be downward and the EIA structure disappeared in general. So, the above-discussed causality is not valid and the nighttime neutral temperature response should be different. The increased Joule heating related to the weakening of the geomagnetic field might be responsible. Hence, the geomagnetic variation would redistribute the temperature in the daytime and nighttime differently (Figure 6), then caused the day-night difference in Figures 6 and 7. The seasonal dependence of the day-night difference in temperature response to the geomagnetic variation is still puzzled and needs further explanation in the future. The temperature redistribution due to geomagnetic variation then causes the tidal responses in Figures 8 and 9. At mid-latitudes, both DW1 and SW2 manifest to be positively correlated to the diploe moment, partly

https://doi.org/10.5194/egusphere-2023-234
Preprint. Discussion started: 15 February 2023

because the strengthen geomagnetic field leading to the lower thermosphere (Cai et al., 2023) modulated the tidal propagation from below. At the low-latitudes, the effect from **E**×**B** drift at daytime becomes important as aforementioned, therefore different from that in mid-latitudes.

As a tentative investigation of the long-term change of thermospheric dynamics during ~12,000 yrs, this paper still has some limitations and flaws, and one of them is the fixed lower boundary. In the present work, the migrating tides at the lower boundary (90 km) are set to be unvaried regardless of simulating different periods in the Holocene. To our knowledge, the long-term trend around mesopause is still debated, and the understanding changed from no trend to a mild negative trend in general (Beig, 2003; Huang et al., 2014; Laštovička, 2017). This is partly because the temperature trends at these heights are sensitive to the changes in stratospheric ozone concentration (Lübken et al., 2013). A whole atmosphere simulation performed by Solomon et al (2018) also indicated there are very weak trends in the mesopause region. Hence, the perpetual lower boundary should be a conservative and compromised treatment, additionally considering little evidences have been provided on how the atmospheric tides change during such a long-term historical time. Besides, the fixed lower boundary inferred that the tidal source from the lower atmosphere is constrained to be unvaried, so our results mainly describe the effect of propagation conditions and local excitation on the long-term dynamics change in the thermosphere. In the next step, simulation based on a whole atmosphere climate model, like the WACCM-X (Liu et al., 2018) and GAIA (Jin et al., 2011), should give a much more realistic scenario of the long-term change in the thermospheric dynamics, nevertheless, the computation cost will increase substantially.

In addition, the empirical model describing the high-latitude input, Weimer-96, is based on modern satellite measurements. Although the geomagnetic intensity variation did not take into consideration, the effect of the geomagnetic tilted angle is included in the model. The drift of magnetic poles and aurora region is thus considered given the Weimer-96 is based on a magnetic coordinate. The intensity of the geomagnetic field is examined to influence the magnetosphere configuration and thus expected to affect the energy input to the high-latitude thermosphere (Zhong et al., 2014; Cnossen et al., 2012). Vogt et al. (2009) summarized the potential impact of the geomagnetic field variation on the geospace by modulating the shielding of the energetic charged particles. During the simulated period, the dipole moment (M) is in the 6×10^{22}–1×10^{23} Am^2 range. As the sine of polar cap size (θ) is generally proportional to $M^{-1/6}$, a rough estimation deduces that θ would change by ~3°, within latitudinal resolution (5°) in the model. Theoretical scaling about cross-polar cap potential (Φ), $\Phi \propto M^{1/3}$, inferring that the Φ should varied from 18 to 21 kV during the Holocene if we set the Φ as 20 kV at the present era. Comparing a typical geomagnetically disturbed condition that Φ is ~80 kV for Kp = 4, the relative change in Φ above is quite small. Cnossen et al. (2014) also declared that the magnetosphere-ionosphere coupling only significantly during the disturbed conditions. Given our

https://doi.org/10.5194/egusphere-2023-234
Preprint. Discussion started: 15 February 2023

simulation is perpetually geomagnetically quiescent, the impact of geomagnetic variation on the high-latitude energy input should be limited.

In this work, the CO2 and geomagnetic fields were regarded as two independent external driving to the simulation regardless of their interaction, although whether the interaction exists is still controversial. Zhou et al. (2021) proposed that the decrease in geomagnetic intensity would redistribute the CO2 in the upper atmosphere using the whole atmosphere simulation. Their investigation suggested that the increased ionospheric conductivities due to the weakened geomagnetic intensity would induce much more Joule heating to warm the high-latitude lower thermosphere, which then should enhance the upwelling flow and bring rich CO2 from below. This result is based on the physical fact that the CO2 distribution becomes deviated from the well-mixed equilibrium above the mesopause (~80–90 km) and the time scale of eddy diffusion becomes much larger in the upper atmosphere (Beagley et al., 2010; Rezac et al., 2015), so that the dynamical processes could modulate the CO2 distribution. However, up to date, little observational evidence has been proposed to support the possible link between CO2 and geomagnetic fields. A simulation project conducted by the whole atmosphere model in the next step could provide more information.

Responses of the non-migrating tides to the variation of CO2 and geomagnetic fields were not considered in this paper. The eastward propagating diurnal tides with a zonal wave number of 3 (DE3) should be not much sensitive to the CO2 change, according to the discussion by Liu et al. (2020). This result was expected as the longitudinal variation of CO2 concentration is generally not obvious. On the other hand, geomagnetic fields crucially influence the non-migrating tidal propagation in the upper atmosphere, through the electro-dynamo or parallel-line transport. For example, Jiang et al. (2018) revealed that DE3 tide can induce the longitudinal wavenumber-3 (WN3) structure rather than the should-be WN4 structure through the electro-dynamical coupling with the geomagnetic field. Zhang et al. (2020) proposed that the significant role of parallel-line transport alters the interhemispheric symmetry as the enhanced planetary waves upward propagated during the 2009 sudden stratosphere warming (SSW) event. As the realistic geomagnetic field is much more complicated than the dipole or tilted dipole, a given non-migrating tides propagating into the thermosphere would broaden the spectra of wavenumber. Yue et al. (2013) found that there were complicated longitudinal structures rather than simply the WN3 as the quasi-2-day wave with westward zonal wavenumber 3 propagating into the upper atmosphere. In this future work, the non-migrating tidal response to the long-term variation will be worth studying.

https://doi.org/10.5194/egusphere-2023-234
Preprint. Discussion started: 15 February 2023

5. Conclusions

This paper diagnosed the long-term changes in the thermospheric dynamics caused by the secular variation of CO2 emissions and geomagnetic field during the Holocene, using the global coupled thermosphere-ionosphere model, GCITEM-IGGCAS. Two sets of long-term time-slice simulation covering ~12,000 yrs were performed by independently controlling the CO2 level and the configuration of geomagnetic fields, both under the perpetual condition of solar minimum and geomagnetic quiescence. The corresponding changes in the circulation and major solar tides in the thermosphere were then analyzed, and the main results were summarized as follows:

1. The CO2 increase/decrease generally strengthened/weakened the general circulation in the thermosphere simultaneously, and notably a dramatic strengthen in the circulation as the CO2 steeply increases since the industrial revolution. The circulation increase due to the CO2 variation was examined to be non-linearly growth, which is expected to be caused by the nonlinear relationship between temperature and molecular viscosity.

2. The amplitude of the diurnal migrating tide in the thermosphere will strengthen as the CO2 increases throughout the Holocene because the increased CO2 cooling provides a plausible condition for tidal propagation.

3. Secular variation of geomagnetic field have a regional impact on the thermospheric circulation, particularly pronounced at high latitudes and around the dusk sector. The prominent hemispheric differences in the thermospheric circulation response infer a crucial role of the geomagnetic non-dipole component.

4. Geomagnetic variations also redistribute neutral temperature at mid- and low-latitudes and lead to different responses in the daytime and nighttime, which then influence the thermospheric dynamics.

5. The geomagnetic dipole moment is highly correlated DW1 tidal amplitude at mid- and low-latitudes during March, and an enhancement of 1×10^{22} Am^2 will cause an increase in ~1–3 K of DW1-T in the thermosphere.

Data availability

The spherical harmonic coefficients of CALS10k.2 model was obtained from the website: https://earthref.org/ERDA/2207. The IGRF model was downloaded from the website: https://www.ngdc.noaa.gov/IAGA/vmod/igrf.html. The Antarctica Vostok and EPICA Dome C ice cores CO2 level was derived from the website: https://data.noaa.gov/dataset/dataset/noaa-wds-paleoclimatology-aicc2012-800kyr-antarctic-ice-core-chronology.The Antarctica Law Dome ice core CO2 data was downloaded from the website: https://www.ncei.noaa.gov/access/metadata/landing-page/bin/iso?id=noaa-icecore-9959. The Mauna Loa observed CO2 was from the website: https://gml.noaa.gov/ccgg/trends/data.html. The simulated data by GCITEM-IGGCAS model under different control runs are available at: http://doi.org/10.17605/OSF.IO/ZQ8HY.

Acknowledgments

The authors acknowledge the support of the B-type Strategic Priority Program of the Chinese Academy of Sciences (Grant XDB41000000), the Project of Stable Support for Youth Team in Basic Research Field, CAS (YSBR-018), the National Natural Science Foundation of China (41621004, 42241106, 42204165), the CAS Youth Interdisciplinary Team (JCTD-2021-05), and the Key Research Program of the Institute of Geology and Geophysics, CAS (Grant IGGCAS-201904).

References

Akmaev, R. A., and Fomichev, V. I.: A model estimate of cooling in the mesosphere and lower thermosphere due to the CO2 Increase over the last 3–4 decades, Geophys. Res. Lett., 27(14), 2113–2116, https://doi.org/https://doi.org/10.1029/1999GL011333, 2000

Akmaev, R. A., Fomichev, V. I., and Zhu, X.: Impact of middle-atmospheric composition changes on greenhouse cooling in the upper atmosphere, J. Atmos. Sol.-Terr. Phys., 68(17), 1879-1889, https://doi.org/https://doi.org/10.1016/j.jastp.2006.03.008, 2006

Alken, P., Thébault, E., Beggan, C. D., Amit, H., Aubert, J., Baerenzung, J., Bondar, T. N., Brown, W. J., Califf, S., Chambodut, A., Chulliat, A., Cox, G. A., Finlay, C. C., Fournier, A., Gillet, N., Grayver, A., Hammer, M. D., Holschneider, M., Huder, L., Hulot, G., Jager, T., Kloss, C., Korte, M., Kuang, W., Kuvshinov, A., Langlais, B., Léger, J. M., Lesur, V., Livermore, P. W., Lowes, F. J., Macmillan, S., Magnes, W., Mandea, M., Marsal, S., Matzka, J., Metman, M. C., Minami, T., Morschhauser, A., Mound, J. E., Nair, M., Nakano, S., Olsen, N., Pavón-Carrasco, F. J., Petrov, V. G., Ropp, G., Rother, M., Sabaka, T. J., Sanchez, S., Saturnino, D., Schnepf, N. R., Shen, X., Stolle, C., Tangborn, A., Tøffner-Clausen, L., Toh, H., Torta, J. M., Varner, J., Vervelidou, F., Vigneron, P., Wardinski, I., Wicht, J., Woods, A., Yang, Y., Zeren, Z., and Zhou, B.: International Geomagnetic Reference Field: the thirteenth generation, Earth, Planets Space, 73, 49, https://doi.org/10.1186/s40623-020-01288-x, 2021.

Beagley, S. R., Boone, C. D., Fomichev, V. I., Jin, J. J., Semeniuk, K., McConnell, J. C., and Bernath, P. F.: First multi-year occultation observations of CO2 in the MLT by ACE satellite: observations and analysis using the extended CMAM, Atmos. Chem. Phys., 10, 1133–1153, https://doi.org/10.5194/acp-10-1133-2010, 2010.

Beig, G., Keckhut, P., Lowe R. P., et al.: Review of mesospheric temperature trends, Rev. Geophys., 41(4), 1015, https://doi.org/10.1029/2002RG000121, 2003

Cai, Y., Yue, X., Wang, W., Zhang, S., Liu, L., Liu, H., & Wan, W.: Long-term trend of topside ionospheric electron density derived from DMSP data during 1995–2017, J. Geophys. Res.: Space Phys., 124, 10708– 10727, https://doi.org/10.1029/2019JA027522, 2019

Cnossen, I.: The importance of geomagnetic field changes versus rising CO2 levels for long-term change in the upper atmosphere, J. Space Weather Space Clim., 4, A18, https://doi.org/10.1051/swsc/2014016, 2014.

Cnossen, I.: A Realistic Projection of Climate Change in the Upper Atmosphere Into the 21st Century, Geophys. Res. Lett., 49, e2022GL100693, https://doi.org/10.1029/2022gl100693, 2022.

https://doi.org/10.5194/egusphere-2023-234
Preprint. Discussion started: 15 February 2023

Cnossen, I. and Maute, A.: Simulated Trends in Ionosphere-Thermosphere Climate Due to Predicted Main Magnetic Field Changes From 2015 to 2065, J. Geophys. Res.: Space Phys., 125, e2019JA027738, https://doi.org/10.1029/2019ja027738, 2020.

Cnossen, I., and Richmond, A. D.: How changes in the tilt angle of the geomagnetic dipole affect the coupled magnetosphere-ionosphere-thermosphere system, J. Geophys. Res. Atmospheres, 117(A10), A10317, https://doi.org/10.1029/2012JA018056, 2012.

Cnossen, I., Richmond, A. D., and Wiltberger, M.: The dependence of the coupled magnetosphere-ionosphere-thermosphere system on the Earth's magnetic dipole moment, J. Geophys. Res.: Space Phys., 117, A05302, https://doi.org/10.1029/2012JA017555, 2012.

Constable, C., Korte, M., and Panovska, S.: Persistent high paleosecular variation activity in southern hemisphere for at least 10 000 years, Earth Planet. Sci. Lett., 453, 78-86, https://doi.org/10.1016/j.epsl.2016.08.015, 2016.

Elias, A. G., de Haro Barbas, B. F., Zossi, B. S., Medina, F. D., Fagre, M., and Venchiarutti, J. V.: Review of long-term trends in the equatorial ionosphere due the geomagnetic field secular variations and its relevance to space weather, Atmosphere, 13, 40, https://doi.org/10.3390/atmos13010040, 2022.

Forbes, J. M.: Dynamics of the thermosphere, Journal of the Meteorological Society of Japan, 85, 193-213, https://doi.org/10.2151/jmsj.85B.193, 2007.

Forbes, J. M., and Zhang, X.: Hough Mode Extensions (HMEs) and solar tide behavior in the dissipative thermosphere, J. Geophys. Res.: Space Phys., 127, e2022JA030962, https://doi.org/10.1029/2022JA030962, 2022.

Gu, H., and Du, J.: On the Roles of Advection and Solar Heating in Seasonal Variation of the Migrating Diurnal Tide in the Stratosphere, Mesosphere, and Lower Thermosphere, Atmosphere, 9(11), 440, http://dx.doi.org/10.3390/atmos9110440, 2018.

Huang, F. T., Mayr, H. G., Russell, J. M., III, and Mlynczak, M. G.: Ozone and temperature decadal trends in the stratosphere, mesosphere and lower thermosphere, based on measurements from SABER on TIMED, Ann. Geophys., 32, 935–949, https://doi.org/10.5194/angeo-32-935-2014, 2014.

IPCC: Climate Change 2014: Synthesis Report. Contribution of Working Groups I, II and III to the Fifth Assessment Report of the Intergovernmental Panel on Climate Change [Core Writing Team, R.K. Pachauri and L.A. Meyer (eds.)]. IPCC, Geneva, Switzerland, 151 pp., 2014.

Jiang, J., Wan, W., Ren, Z., and Yue, X.: Asymmetric de3 causes wn3 in the ionosphere, J. Atmos. Sol.-Terr. Phys., 173, 14-22, http://dx.doi.org/10.1016/j.jastp.2018.04.006, 2018.

Jin, H., Miyoshi, Y., Fujiwara, H., Shinagawa, H., Terada, K., and Terada, N., et al.: Vertical connection from the tropospheric activities to the ionospheric longitudinal structure simulated by a new Earth's whole atmosphere-ionosphere coupled model, J. Geophys. Res., 116(A1), A01316, https://doi.org/10.1029/2010JA015925, 2011.

Keeling, C. D., Whorf, T. P., Wahlen, M., & vander Plicht, J. : Interannual extremes in the rate of rise of atmospheric carbon dioxide since 1980, Nature, 375(6533), 666–670, https://doi.org/10.1038/375666a0, 1995.

Kogure, M., Liu, H., and Tao, C.: Mechanisms for zonal mean wind responses in the thermosphere to doubled CO2 concentration, J. Geophys. Res.: Space Phys., 127, e2022JA030643, https://doi.org/10.1029/2022JA030643, 2022

https://doi.org/10.5194/egusphere-2023-234
Preprint. Discussion started: 15 February 2023

Korte, M., Constable, C., Donadini, F., and Holme, R.: Reconstructing the Holocene geomagnetic field, Earth and Planetary Science Letters, 312(3–4), 497–505, https://doi.org/10.1016/j.epsl.2011.10.031, 2011

Laštovička, J., R. Akmaev, A., Beig, G., Bremer, J., and Emmert J. T.: Global change in the upper atmosphere, Science, 314, 1253-1254, https://doi.org/10.1126/science.1135134, 2006.

Laštovička, J.: A review of recent progress in trends in the upper atmosphere, J. Atmos. Sol.-Terr. Phys., 163, 2-13, https://doi.org/10.1016/j.jastp.2017.03.009, 2017.

Liu, H., Tao, C., Jin, H., and Nakamoto, Y.: Circulation and tides in a cooler upper atmosphere: Dynamical effects of CO2 doubling, Geophys. Res. Lett., 47, e2020GL087413. https://doi.org/10.1029/2020GL087413, 2020

Liu, H.-L., Bardeen, C. G., Foster, B. T., Lauritzen, P., Liu, J., Lu, G., ... Wang, W.: Development and validation of the Whole Atmosphere Community Climate Model with thermosphere and ionosphere extension (WACCM-X 2.0), J. Adv. Model. Earth Syst., 10, 381–402, https://doi.org/10.1002/2017MS001232, 2018

Lübken, F.-J., Berger, U., and Baumgartner, G.: Temperature trends in the midlatitude summer mesosphere. J. Geophys. Res.: Atmospheres, 118, 13347–13360, https://doi.org/10.1002/2013JD020576, 2013.

Lüthi, D., Le Floch, M., Bereiter, B., Blunier, T., Barnola, J.-M., Siegenthaler, U., et al.: High-resolution carbon dioxide concentration record 650,000–800,000 yr before present, Nature, 453, 379–382, https://doi.org/10.1038/nature06949, 2008.

MacFarling Meure, C., Etheridge, D., Trudinger, C., Steele, P., Langenfelds, R., van Ommen, T., et al.: Law Dome CO2, CH4, and N2O ice core records extended to 2,000 yr BP, Geophys. Res. Lett., 33, L14810, https://doi.org/10.1029/2006GL026152, 2006.

Marsh, D. R., Mills, M. J., Kinnison, D. E., Lamarque, J. F., Calvo, N., and Polvani, L. M.: Climate change from 1850 to 2005 simulated in CESM1(WACCM), J. Climate, 26(19), 7372–7391, https://doi.org/10.1175/JCLI-D-12-00558.1, 2013.

Neale, R. B., Richter, J., Park, S., Lauritzen, P. H., Vavrus, S. J., Rasch, P. J., and Zhang, M. H.: The mean climate of the Community Atmosphere Model (CAM4) in forced SST and fully coupled experiments, J. Climate, 26(14), 5150–5168. https://doi.org/10.1175/JCLI-D-12-00236.1, 2013.

Oberheide, J., Forbes, J. M., Häusler, K., Wu, Q., and Bruinsma, S. L.: Tropospheric tides from 80 to 400 km: Propagation, interannual variability, and solar cycle effects, J. Geophys. Res.: Atmosphere. 114, D00I05, https://doi.org/10.1029/2009JD012388, 2009.

Ogawa, Y., Motoba, T., Buchert, S. C., Häggström, I., and Nozawa, S.: Upper atmosphere cooling over the past 33 yr, Geophys. Res. Lett., 41, 5629–5635, https://doi.org/10.1002/2014GL060591, 2014

Qian, L., Laštovička, J., Roble, R. G., and Solomon, S. C.: Progress in observations and simulations of global change in the upper atmosphere, J. Geophys. Res.: Space Phys., 116, A00H03, https://doi.org/10.1029/2010JA016317, 2011.

Qian, L., Roble, R. G., Solomon, S. C., and Kane, T. J.: Calculated and observed climate change in the thermosphere, and a prediction for solar cycle 24, Geophys. Res. Lett., 33, L23705, https://doi.org/10.1029/2006gl027185, 2006.

Qian, L. Y., Burns, A. G., Solomon, S. C., and Wang, W. B.: Carbon dioxide trends in the mesosphere and lower thermosphere, J. Geophys. Res., 122(4), 4474–4488, https://doi.org/10.1002/2016JA023825, 2017.

https://doi.org/10.5194/egusphere-2023-234
Preprint. Discussion started: 15 February 2023

Rezac, L., Jian, Y., Yue, J., Russell III, J. M., Kutepov, A., Garcia, R., Walker, K., and Bernath, P.: Validation of the global distribution of CO2 volume mixing ratio in the mesosphere and lower thermosphere from SABER, J. Geophys. Res., 120(23), 12067–12081, https://doi.org/10.1002/2015JD023955, 2015

Ren, Z., Wan, W., and Liu, L.: GCITEM-IGGCAS: A new global coupled ionosphere–thermosphere-electrodynamics model, J. Atmos. Sol.-Terr. Phys., 71, 2064-2076, https://doi.org/10.1016/j.jastp.2009.09.015, 2009.

Ren, Z., Wan, W., Liu, L., and Xiong, J.: Simulated longitudinal variations in the lower thermospheric nitric oxide induced by nonmigrating tides, J. Geophys. Res.: Space Phys., 116, A04301, https://doi.org/10.1029/2010ja016131, 2011.

Ren, Z., Wan, W., Xiong, J., and Li, X.: A Simulation of the Influence of DE3 Tide on Nitric Oxide Infrared Cooling, J. Geophys. Res.: Space Phys., 125, e2019JA027131, https://doi.org/10.1029/2019ja027131, 2020.

Ren, Z., Wan, W., Xiong, J., and Liu, L.: Simulated wave number 4 structure in equatorial F-region vertical plasma drifts, J. Geophys. Res.: Space Phys., 115, A05301, https://doi.org/10.1029/2009ja014746, 2010.

Richmond, A. D.: Ionospheric Electrodynamics Using Magnetic Apex Coordinates, J. Geomagn. Geoelectr., 47, 191-212, https://doi.org/10.5636/jgg.47.191, 1995.

Rind, D., Suozzo, R., Balachandran, N. K., and Prather, M. J.: Climate change and the middle atmosphere Part I: The doubled CO2 climate, J. Atmos. Sci., 47(4), 475–494, https://doi.org/10.1175/1520-0442(1998)011<0876:CCATMA>2.0.CO;2, 1990.

Roble, R. G. and Dickinson, R. E.: How will changes in carbon dioxide and methane modify the mean structure of the mesosphere and thermosphere?, Geophys. Res. Lett., 16, 1441-1444, https://doi.org/10.1029/GL016i012p01441, 1989.

Roble, R. G., Ridley, E. C., Richmond, A. D., & Dickinson, R. E.: A coupled thermosphere/ionosphere general circulation model, Geophys. Res. Lett., 15(12), 1325–1328, https://doi.org/10.1029/gl015i012p01325, 1988

Solomon, S. C., Liu, H. L., Marsh, D. R., McInerney, J. M., Qian, L., and Vitt, F. M.: Whole Atmosphere Simulation of Anthropogenic Climate Change, Geophys. Res. Lett., 45(3), https://doi.org/10.1002/2017GL076950, 2018.

Solomon, S. C., Qian, L., and Roble, R. G.: New 3-D simulations of climate change in the thermosphere, J. Geophys. Res.: Space Phys., 120(3), 2183-2193, https://doi.org/10.1002/2014ja020886, 2015

Sun, R., Gu, S., Dou, X., and Li, N.: Tidal Structures in the Mesosphere and Lower Thermosphere and Their Solar Cycle Variations, Atmosphere, 13(12), 2036, http://dx.doi.org/10.3390/atmos13122036, 2022

Vogt, J., Sinnhuber, M., Kallenrode, MB.: Effects of Geomagnetic Variations on System Earth, in: Geomagnetic Field Variations, Advances in Geophysical and Environmental Mechanics and Mathematics, Springer, Berlin, Heidelberg, https://doi.org/10.1007/978-3-540-76939-2_5, 2009.

Weimer, D. R.: A flexible, IMF dependent model of high-latitude electric potentials having "space weather" applications, Geophys. Res. Lett., 23(18). https://doi.org/10.1029/96GL02255, 1996

Yue, J., Wang, W., Richmond, A. D., Liu, H.-L., and Chang, L. C.: Wavenumber broadening of the quasi 2 day planetary wave in the ionosphere, J. Geophys. Res.: Space Phys., 118, 3515–3526, https://doi.org/10.1002/jgra.50307, 2013

Yue, X., Cai, Y., Ren, Z., Zhou, X., Wei, Y., and Pan, Y.: Simulated Long-Term Evolution of the Ionosphere During the Holocene, J. Geophys. Res.: Space Phys., 127, e2022JA031042, https://doi.org/10.1029/2022ja031042, 2022.

https://doi.org/10.5194/egusphere-2023-234
Preprint. Discussion started: 15 February 2023

Yue, X., Hu, L., Wei, Y., Wan, W., and Ning, B.: Ionospheric trend over Wuhan during 1947–2017: Comparison between simulation and observation, J. Geophys. Res.: Space Phys., 123, 1396–1409, https://doi.org/10.1002/2017JA024675, 2018

Zhang, S.-R., Holt, J. M., Erickson, P. J., Goncharenko, L. P., Nicolls, M. J., McCready, M., and Kelly, J.: Ionospheric ion temperature climate and upper atmospheric long-term cooling, J. Geophys. Res.: Space Phys., 121, 8951–8968. https://doi.org/10.1002/2016JA022971, 2016

Zhang, R., Liu, L., Liu, H., Le, H., Chen, Y., and Zhang, H.: Interhemispheric transport of the ionospheric F region plasma during the 2009 sudden stratosphere warming, Geophys. Res. Lett., 47, e2020GL087078, https://doi.org/10.1029/2020GL087078, 2020

Zhou, X., Yue, X. A., Liu, H. L., Wei, Y., and Pan, Y. X.: Response of atmospheric carbon dioxide to the secular variation of weakening geomagnetic field in whole atmosphere simulations, Earth and Planetary Physics, 5(4), 327–336, https://doi.org/10.26464/epp2021040, 2021

Zhou, X., Yue, X., Ren, Z., Liu, Y., Cai, Y., Ding, F., and Wei, Y.: Impact of Anthropogenic Emission Changes on the Occurrence of Equatorial Plasma Bubbles, Geophys. Res. Lett., 49, e2021GL09735, https://doi.org/10.1029/2021gl097354, 2022.

Zhong, J., Wan, W. X., Wei, Y., Fu, S. Y., Jiao, W. X., Rong, Z. J., et al.: Increasing exposure of geosynchronous orbit in solar wind due to decay of Earth's dipole field, J. Geophys. Res.: Space Phys., 119, 9816–9822, https://doi.org/10.1002/2014JA020549, 2014

Zossi, B. S., Elias, A. G., and Fagre, M.: Ionospheric conductance spatial distribution during geomagnetic field reversals, J. Geophys. Res., 123(3), 2379–2397, https://doi.org/10.1002/2017JA024925, 2018

https://doi.org/10.5194/egusphere-2023-234
Preprint. Discussion started: 15 February 2023

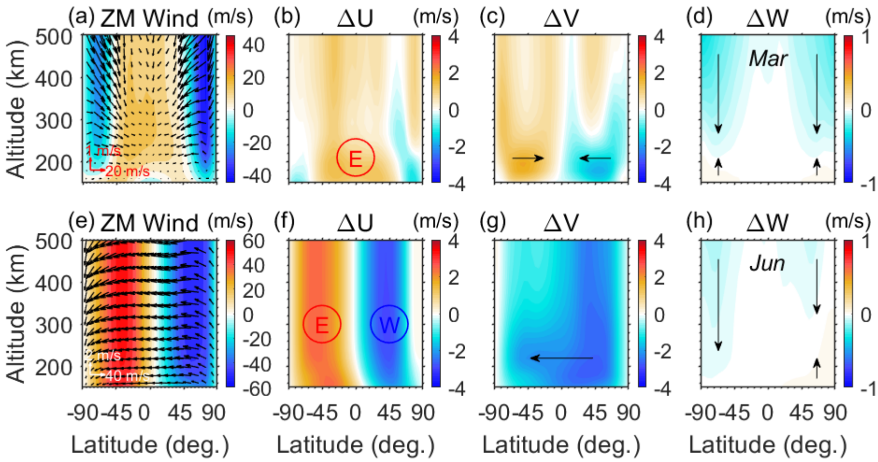

Figure 1. (a) Thermospheric circulation is illustrated by contours (zonal) and arrays (meridional and vertical) in March 2015. (b)–(d) Changes in zonal, meridional and vertical wind velocity due to the increase of CO2 from 1945 to 2015. Plots (e)–(f) are the same as plots (a)–(d) but for June.

https://doi.org/10.5194/egusphere-2023-234
Preprint. Discussion started: 15 February 2023

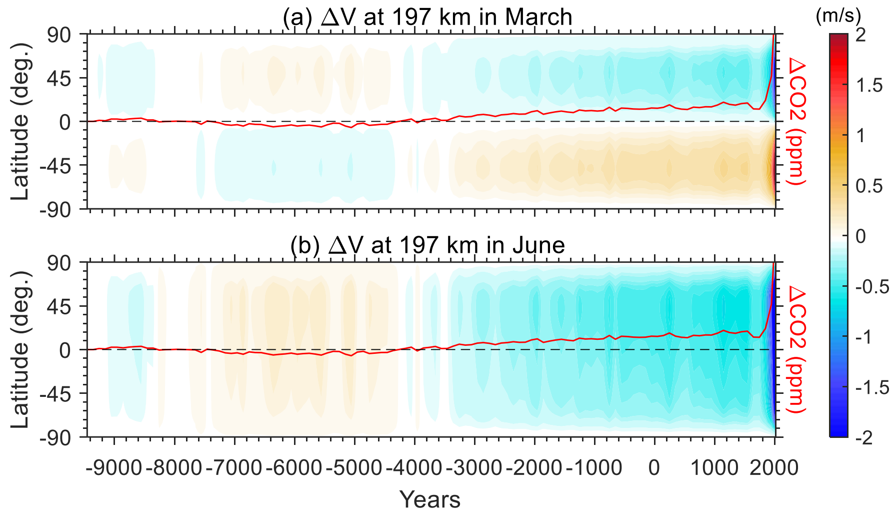

492

493 **Figure 2.** Time evolution of the changes in the zonal-mean meridional wind at 197 km during (a) March and (b) June. The
494 corresponding CO2 variation is plotted in the red solid line.

495

496

https://doi.org/10.5194/egusphere-2023-234
Preprint. Discussion started: 15 February 2023

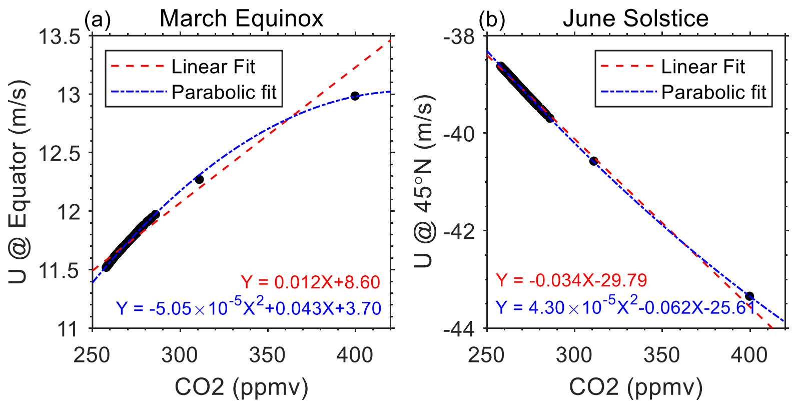

Figure 3. Response of thermospheric zonal-mean zonal winds (150–600 km average) to the CO_2 increase (a) at the equator in the March equinox. (b) at 45°N in the June solstice. Linear and parabolic fitting are indicated in red-dashed and blue-dash-dotted lines, respectively.

https://doi.org/10.5194/egusphere-2023-234
Preprint. Discussion started: 15 February 2023

502 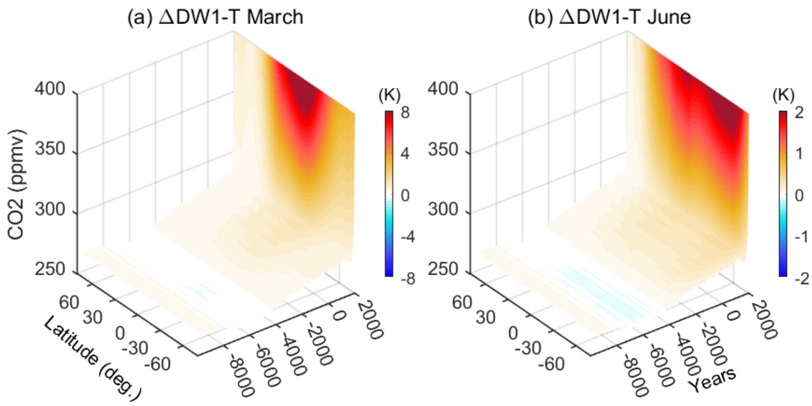

503 **Figure 4.** Change in the amplitude of diurnal migrating tide (DW1) at 240 km due to the CO2 variation in (a) March and (b)
504 June with respect to the beginning of the simulation.

505

https://doi.org/10.5194/egusphere-2023-234
Preprint. Discussion started: 15 February 2023

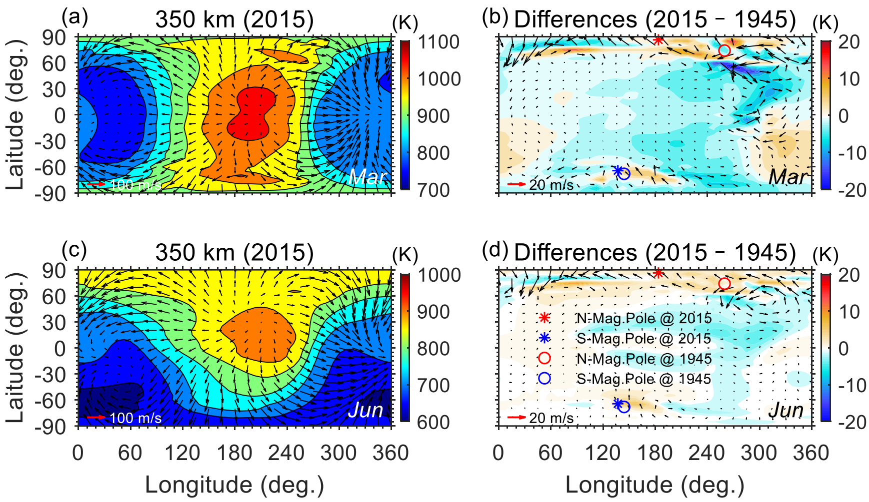

Figure 5. Geographic distribution of neutral temperature (color contours,) and horizontal winds (black arrows) at 350 km in (a) March and (c) June at UT00. (b) Differences in neutral temperature and horizontal winds due to changes in geomagnetic field between 1945 and 2015. The scales of wind velocity are indicated in the lower-left corner of each plot. The changes of north and south magnetic poles between 1945 and 2015 are illustrated in plots (b) and (d).

https://doi.org/10.5194/egusphere-2023-234
Preprint. Discussion started: 15 February 2023

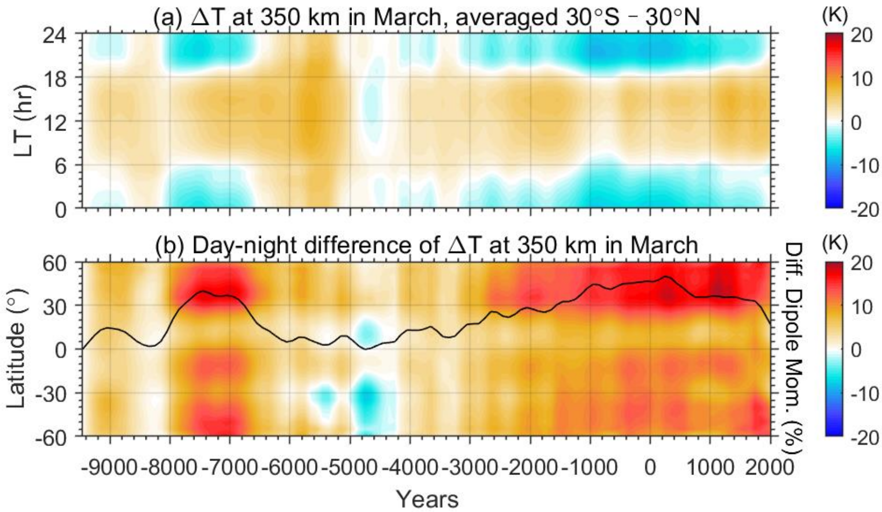

Figure 6. (a) Local-time (LT) variation of the zonal-mean temperature changes at low latitudes (30°S–30°N) caused by the secular variation of geomagnetic fields at 350 km in March during the Holocene. (b) Latitudinal variation of day-night differences in the zonal-mean temperature during March plotted versus year and with respect to the beginning of the simulation. The daytime and nighttime are corresponding to LT10–14 and LT22–02, respectively. Relative change of the geomagnetic dipole moment is plotted in the black-solid line in plot (b).

https://doi.org/10.5194/egusphere-2023-234
Preprint. Discussion started: 15 February 2023

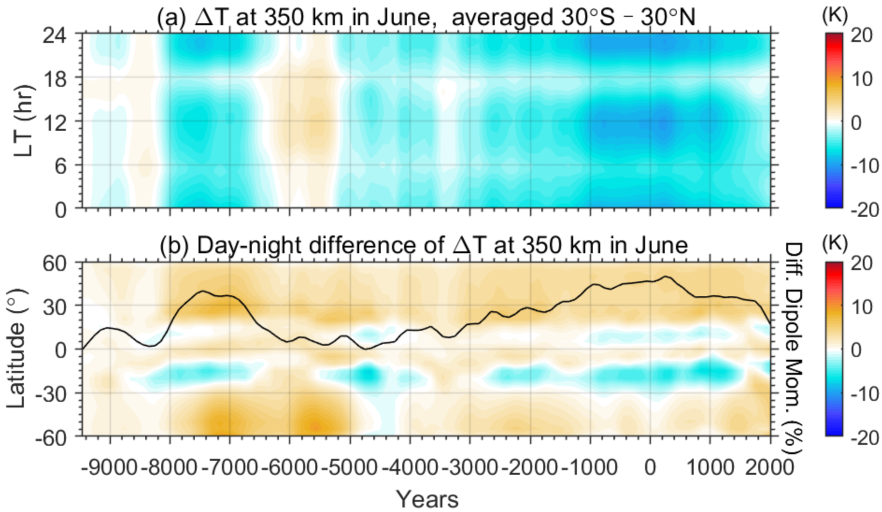

519

520 **Figure 7.** Same as Figure 6, but for the case of June.

521

https://doi.org/10.5194/egusphere-2023-234
Preprint. Discussion started: 15 February 2023

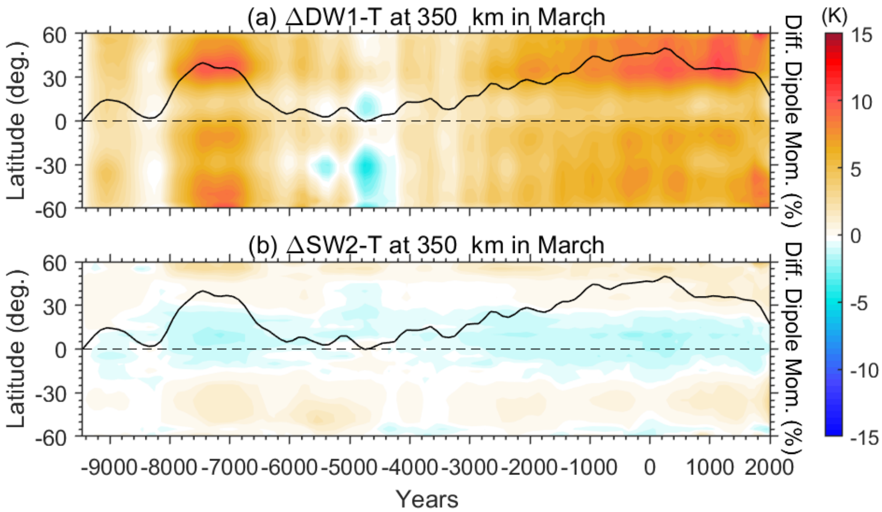

Figure 8. Time evolution of the differences in the amplitude of (a) DW1 and (b) SW2 with respect to the beginning of the simulation.

https://doi.org/10.5194/egusphere-2023-234
Preprint. Discussion started: 15 February 2023

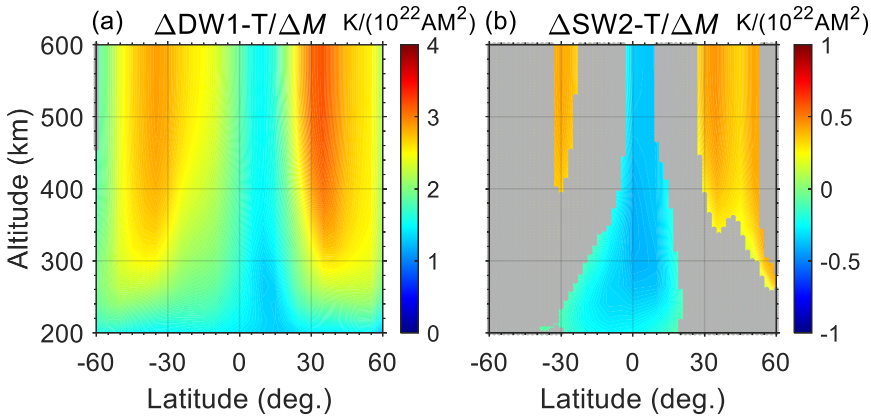

Figure 9. Regression of (a) DW1-T and (b) SW2-T amplitudes on the geomagnetic dipole moment. The grey shaded area indicates where the absolute values of correlation coefficients are less than 0.6.